JOURNAL OF AIRCRAFT
Vol. 45, No. 2, March–April 2008

Aerodynamic Characteristics of a Gurney/Jet Flap at Low Reynolds Numbers

Lance W. Traub*
Embry-Riddle Aeronautical University, Prescott, Arizona 86301-3720
and
Gaurav Agarwal†
Texas A&M University, College Station, Texas 77843-3141

DOI: 10.2514/1.28016

A low-speed wind-tunnel investigation has been undertaken to establish the effect of a Gurney flap used in conjunction with a jet flap at low Reynolds numbers. The characteristics of the combination were explored as a potential control effector for small unmanned aerial vehicles. Measurements included force balance, wake survey, and flow visualization. The results indicate that the jet flap maintains a theoretically determined dependence on the jet momentum coefficient, even at a low Reynolds number (160,000). A numerical lifting-line program was modified to allow estimate of the rolling moment that may be generated by ailerons composed of a Gurney/jet flap. The numerical data suggest that the jet flap is capable of generating significant rolling moments with realistic jet momentum coefficients.

Nomenclature

A_n	=	Fourier coefficient
AR	=	aspect ratio
b	=	wing span
C_L	=	lift coefficient
Cl	=	sectional lift coefficient
C_l	=	rolling moment coefficient
Cmu	=	jet momentum coefficient
c	=	chord
N	=	numerical index, number of spanwise evaluation locations
U	=	velocity
y	=	spanwise coordinate
y_o	=	spanwise evaluation point
q	=	dynamic pressure
q_o	=	freestream dynamic pressure
α	=	angle of attack
η	=	nondimensional spanwise coordinate
Γ	=	circulation

Subscripts

eff	=	effective
geo	=	geometric
i	=	induced
inf	=	infinity (freestream)
te	=	trailing edge
ZL	=	zero lift

Introduction

EVER-INCREASING application has driven a significant research effort to extend, refine, and hone the available technological toolbox for unmanned aerial vehicles (UAVs). UAV mission effectiveness, coupled with comparatively low cost and flexibility, makes this type of vehicle extremely attractive. UAVs range from the disposable to the sophisticated (Global Hawk). Interest in enhanced stealth potential for this type of vehicle has spurred the development of suitable enabling technologies.

Flight vehicle lateral and longitudinal control is typically affected through the use of a movable surface, usually an aileron or elevator. From a stealth perspective, any control surface that creates a discontinuity in the wing form may serve as a radar reflection source. A natural way to eliminate this problem is to remove the conventional control surfaces. A well-proven technology to this end is the jet flap. A jet flap functions by ejecting a high-velocity sheet of air from the airfoil's trailing edge. The jet is typically inclined relative to the trailing edge and augments lift by creating a finite pressure difference at the trailing edge. As shown by Spence's analysis [1], lift augmentation has two components: one due to an effective lengthening of the airfoil (requires significant jet momentum) and one due to the inclination of the jet (greater turning of the flow: a cambering effect).

Recent research efforts have indicated that a small-scale trailing-edge control effector, the Gurney flap, can achieve significant lift modulation while structurally representing only a minor modification. The Gurney flap [2,3] is usually a small plate (0.5 to 1.5% of the chord) that is attached at or near the trailing edge of an airfoil on the pressure side. The Gurney functions by essentially increasing the downward deflection of the trailing-edge flow. Pressure measurement studies have indicated an apparent violation of the trailing-edge Kutta condition; experimental data show that finite loading is carried to the trailing edge. The Gurney flap increases the effective chord and camber of the airfoil, thereby augmenting circulation. Liebeck [4] suggested a flow pattern in which a virtual cusped trailing edge is formed downstream of the Gurney from the shear layers merging downstream of the flap. The final pressure recovery would then occur offsurface, which is analogous to a violation of the Kutta condition. Investigation [5] has also indicated that the drag increment associated with this type of flap may be lessened by creating discontinuities in the flap surface that serve to introduce three-dimensional flow effects into the wake, helping to attenuate the von Kármán vortex street that has been observed to form downstream of the flap. Both the Gurney flap and jet flap represent mature and proven technologies that may prove suitable for stealthy implementation into UAV-type flight vehicles.

Consequently, a study has been undertaken to evaluate the effectiveness of a Gurney/jet flap combination at a Reynolds number typical of what may be seen for a low-speed UAV. The Gurney flap

Received 25 September 2006; revision received 28 November 2006; accepted for publication 22 November 2006.

*Associate Professor, Aerospace Engineering Department. Member AIAA.
†Graduate Student, Aerospace Engineering Department.

may be seen as a mechanical backup to the jet flap, in case of pneumatic failure. The study aims to determine if high Reynolds number behavior is preserved at low Reynolds numbers and that jet flap operational dependencies are maintained.

Equipment and Procedure

The wind-tunnel investigation has been undertaken in Texas A&M University's 1 by 1 ft open-circuit wind tunnel to ascertain the effect of the jet flap in concert with a Gurney flap. Tests were undertaken at a freestream velocity of 20 m/s, yielding a chord-based Reynolds number of 160,000. Because of the comparative nature of the testing, wall effects (blockage and streamline curvature) were not estimated. The test wing was rapid-prototyped in acrylonitrile butadiene styrene (ABS) plastic. The wing has a chord of 122 mm and a span of 140 mm (see Fig. 1). The Gurney flap has a projected height of approximately 1 mm. The flaps inclination is 20 deg from the vertical. Study [6] has indicated that the lift of a Gurney flap scales with the projected flap height perpendicular to the surface. Inclining the flap reduces the minimum drag penalty associated with flap addition [6].

The flap and trailing-edge geometry was chosen to mimic that found on an Extra 330S UAV being tested for hingeless lateral control at Texas A&M University, for which the jet flap/Gurney replaces a conventional aileron. Figure 2 shows details of the UAV jet flap design and its ability to deflect the jet. The design uses a

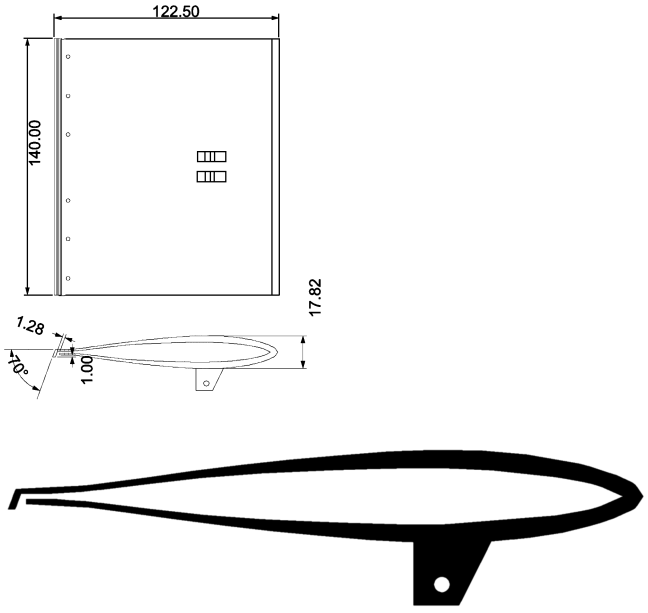

Fig. 1 Sectional view through test model and model geometry, with dimensions in millimeters.

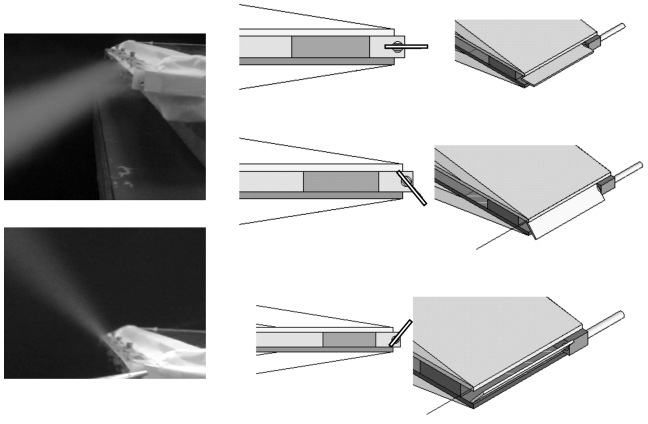

Fig. 2 CAD rendering and fabricated jet exit showing jet deflection using a Gurney flap deflector.

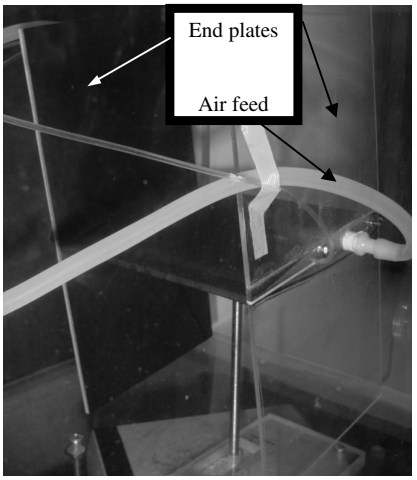

Fig. 3 Test wing installed in the tunnel.

centrally mounted plate to deflect the trailing-edge jet either up or down depending on the nature of the desired lift modulation. Additionally, the plate serves as a 0.75% Gurney flap when inclined at 70 deg. This design approach was implemented because the Gurney flap provides lateral control in the event of pneumatic failure (e.g., low batteries or excessive fan motor temperature). As may be seen, this simple implementation is able to effectively deflect the jet up or down. Note that in the wind-tunnel tests, the baseline wing (no Gurney flap) was formed by fairing in the pressure side surface, using clay. Consequently, the Gurney flap was eliminated. This resulted in a trailing edge that is essentially blunt. A sharp trailing edge was not used for the baseline case, because the model was designed to mimic, as closely as possible, the flight test vehicle configuration shown in Fig. 2, in which the trailing edge would essentially be blunt.

The wing was equipped with end plates to reduce three-dimensional effects. This does not, however, imply that the flow was two-dimensional, due to the limited extent of the side plates. The end plates were manufactured from clear acrylic. The plates were 122 by 246 mm high (see Fig. 3). A Setra EL-4100D force balance was used to acquire the lift data. Considering the low aerodynamic loads, a high-resolution force balance was selected, because this balance can repeatably resolve loads of 0.01 g. Calibration of the balance using certified masses indicated accuracies better than 0.02 g.

The jet exit was surveyed with a stagnation probe to determine velocity uniformity, which was determined to be within 5%. A FlowKinetics™ LLC FKS 1DP-PBM manometer/velocity meter was used to measure the velocities. This instrument is quoted by the manufacturer to have accuracy better than 0.1%. Shop air was used to supply the jet. The internal cavity of the wing served as a plenum, which was pressure-tapped. These pressures were then used to calculate the jet exit velocity. Calculated estimates of the jet exit velocity (using the plenum pressure) were compared against direct measurement (using the stagnation probe) that indicated an error of less then 1.5%. The jet momentum coefficients that were used in the tests were selected to be practically realizable using self-contained modular blowers developed at Texas A&M University.

External air supplies often cause significant difficulties, due to transfer loads from the pressurized tubing onto the model showing up as spurious forces and moments. To mitigate these effects, flexible tubing (silicon) was used. Tare tests were also undertaken (wind-off) to estimate the transmitted loads throughout the tested incidence range. Data indicated that the loads were very low.

Results and Discussion

Force Balance

Figure 4 shows the measured lift coefficient as a function of wing incidence. The data show the traditional trailing-edge cambering effect of both the Gurney flap and the jet flap. Both of these flow effectors essentially displace the lift coefficient curve such that the

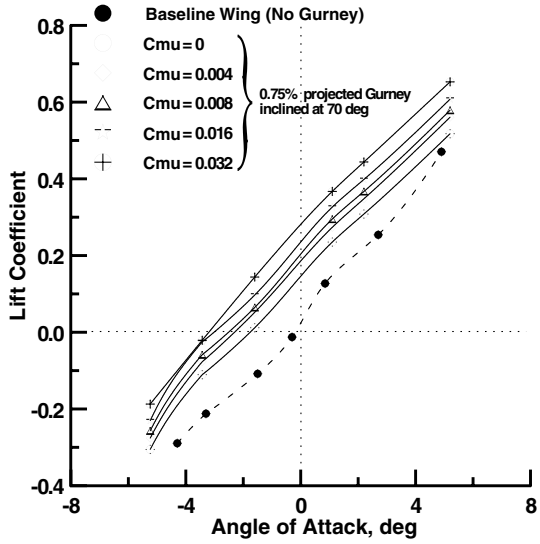

Fig. 4 Effect of the jet flap on the measured lift coefficient.

angle of attack for zero lift is negative. Effects on the lift curve slope (approximately 0.08/ deg) are minimal. Spence's [1] analysis suggests that for the low jet momentum coefficients used in this study, a theoretical maximum increase in the lift curve slope of approximately 3% may occur. This increase, which is independent of the jet flap angle, is due to an effective lengthening of the chord of the airfoil. Final pressure recovery would then occur in the wake when the jet's deflection becomes negligible (i.e., it cannot maintain a pressure differential). Note that balance load limitations precluded examination of wing stall characteristics.

Figure 5 shows a data analysis summary elucidating the effects of pneumatic flow manipulation. The lift augmentation ratio (LAR) is defined as the lift coefficient with jet flap, less no jet flap, divided by the jet momentum coefficient. It is an indicator of how *efficiently* the jet alters the wing lift. Coefficients greater than one illustrate that the lift increment is greater than that due to the pure jet reaction. The data indicate that low Cmu is far more effective at increasing lift efficiently, with a $1/\sqrt{Cmu}$ dependency shown, as suggested by

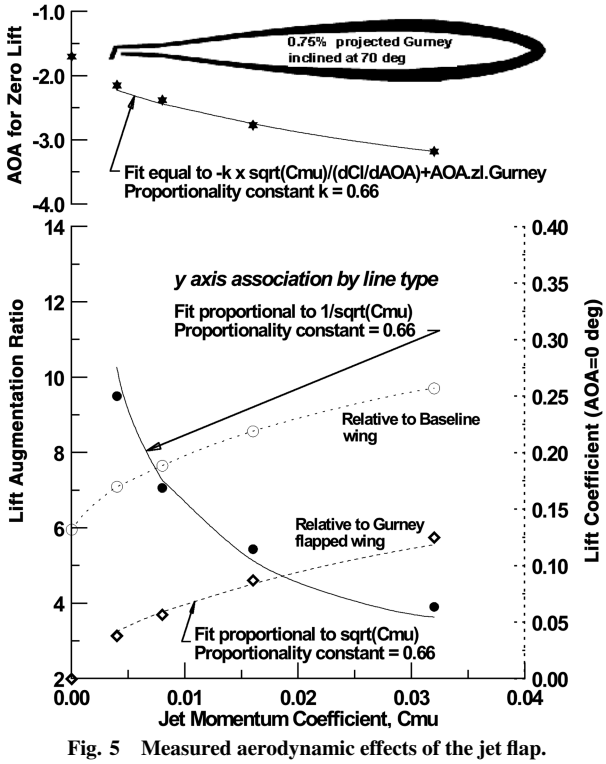

Fig. 5 Measured aerodynamic effects of the jet flap.

theory. Additionally, the increment in the zero angle of attack lift coefficient is seen to vary with $\sqrt{Cmu}$, also as suggested by theory. Thus, increasing the jet momentum coefficient does increase the lift relative to $Cmu = 0$ monotonically, but at a steadily decreasing rate. The data also show an angle of attack negative shift proportional to $\sqrt{Cmu}$ (top inset in Fig. 5). Curve fits to the data yield

$$\alpha_{ZL} = -0.66\sqrt{Cmu}/(\mathrm{d}Cl/\mathrm{d}\alpha) + \alpha_{ZL\ \mathrm{Gurney}} \tag{1}$$

$$\mathrm{LAR} = 0.66/\sqrt{Cmu} \tag{2}$$

$$Cl_{\alpha=0} = 0.66\sqrt{Cmu} + Cl_{\alpha=0\ \mathrm{Gurney}} \tag{3}$$

Wake Survey

To explore the effects of the jet flap on the wake, a survey was conducted downstream of the trailing edge (at two chord lengths downstream), using a small pitot static probe. The survey was conducted as far downstream as possible, to satisfy an assumption in Jones's [7] equation that the static pressure is unperturbed from that upstream of the model. Thus, the profile drag may be estimated using

$$\mathrm{drag\ \ coefficient} = \frac{2}{\mathrm{chord}} \int_{yl}^{yu} \sqrt{\frac{q}{q_o}} - \frac{q}{q_o}\,\mathrm{d}y \tag{4}$$

where yl and yu are integration bounds for the wake survey. The wake was surveyed in 1/12-in. increments. Results are shown for selected test cases in Fig. 6. The data show that the jet flap increases the wake width and maximum velocity defect. Higher lift for a given wing incidence is also reflected in lower wake position relative to the trailing edge. All plots also show a distinct wake asymmetry above and below the point of maximum velocity defect; the defect region is larger below the point of minimum velocity. This may indicate that the lower surface, due to the Gurney presence, contributes a large portion of the total profile drag, possibly due to the formation of a vortex street downstream of the flap. Note that results of other studies [8,9] do not clearly show a wake shape asymmetry as observed in the present study.

Figure 7 shows the integrated velocity profiles [using Eq. (4)] displaying the profile drag coefficient for the test wing. The data indicate that all Gurney/Jet flap test cases recorded lower drag than the baseline wing for a given lift coefficient. Most studies show an increase in the minimum drag coefficient with Gurney attachment; however, in the present study, the baseline wing has a blunt trailing edge (with 3% height to chord), to mimic that of the flight test vehicle. An increase in the minimum drag coefficient is well documented [10] (due to vortex street formation) for blunt trailing edges (although the lift curve slope and maximum lift coefficient may increase [11]). Figure 7 also shows that $Cmu > 0$ causes an increase in the minimum drag coefficient, which also occurs at a higher lift coefficient.

Flow Visualization

Figure 8a shows smoke injection visualization of the trailing-edge jet sheet. Smoke was injected into the bellmouth and positioned to impinge at the leading edge of the airfoil. A laser was then used to create a light sheet to aid in visualization. The jet is seen to turn rapidly downstream; initially due to the imposed pressure gradient across it and then due to entrainment of the freestream streamwise momentum [12]. The jet also diffuses rapidly. To help elucidate the flow physics, a figure reproduced from [13], showing visualization of the streakline pattern due to a jet flap, is included (Fig. 8b). Although not an identical configuration to that tested, the physics should be similar. The jet flap shows evidence of significant turning of the flow around the trailing edge, such that the jet exit becomes functionally the rear separation point. As seen in the smoke, the jet is seen to

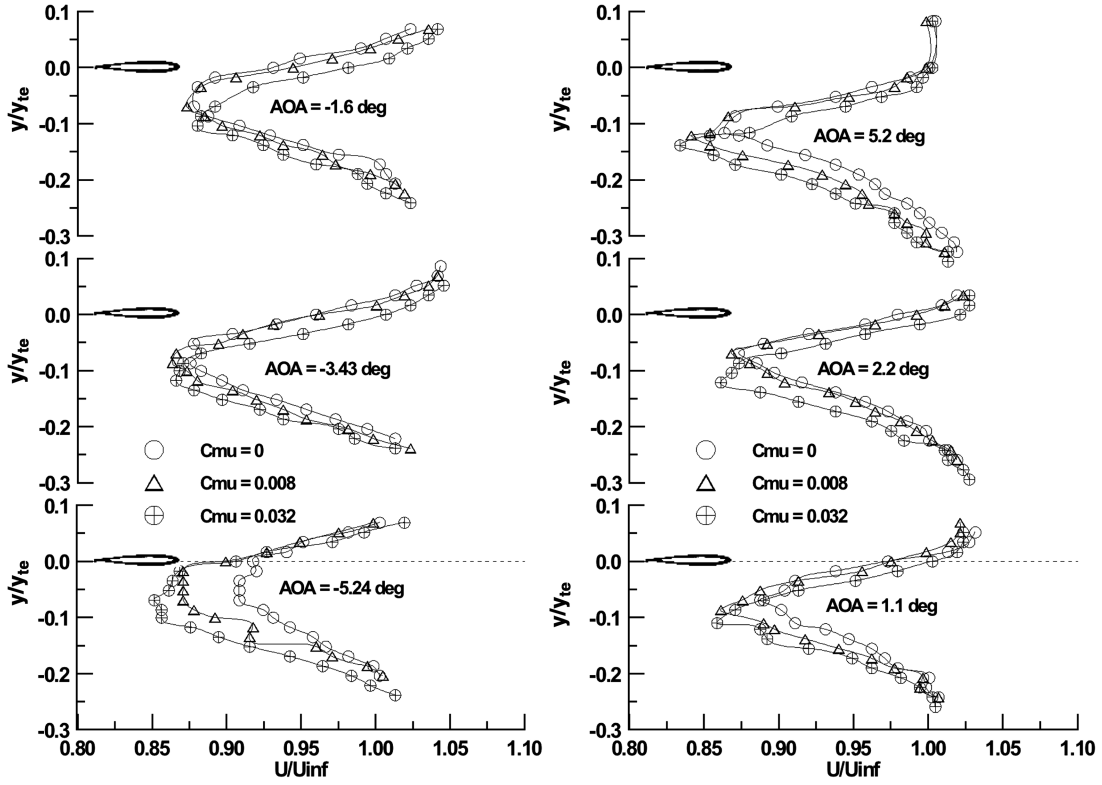

Fig. 6 Measured wake velocity defect profiles.

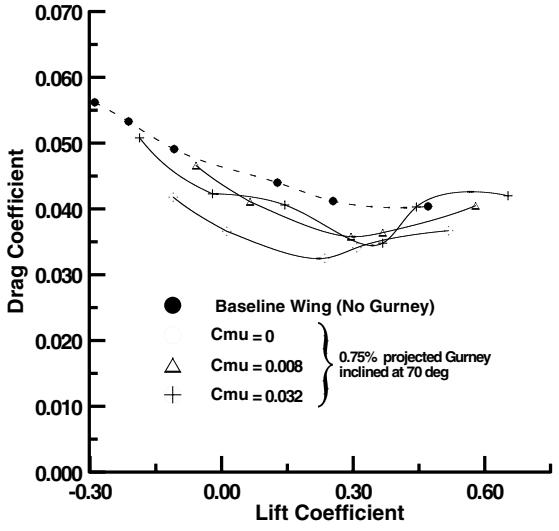

Fig. 7 Effect of jet flap on measured drag coefficient.

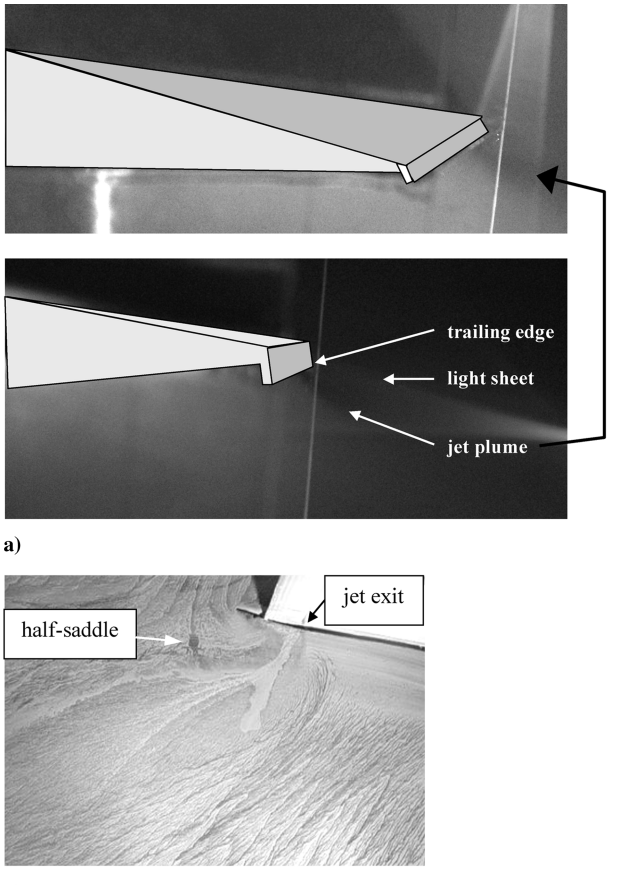

Fig. 8 Smoke flow visualization of the jet plume: a) present test (flow left to right; wing sketch overlay included for clarity) and b) figure reproduced from [15].

expand rapidly and deflect streamwise. Notice the half-saddle aft of the trailing edge, demarcating the dividing streamline between fluid drawn around the trailing edge and that drawn down and streamwise. The skin friction pattern also suggests that the jet flap draws the lower surface boundary layer away from the surface [12].

Rolling Moments

A goal of the present research effort is to establish the suitability of a pneumatic system in achieving hingeless control. Consequently, it would be valuable to establish if the observed lift modulation is capable of generating rolling moments suitable for lateral control. Because the effect of the Gurney/jet flap is analogous to a conventional trailing-edge device, estimation of rolling moments may be made by application of numerical lifting-line theory. For each

tested configuration, the zero lift angle of attack may be determined. This may then be implemented into a lifting-line program and the moments may be estimated.

A comprehensive discussion of numerical lifting-line theory can be found in most aerodynamics texts [14,15]. Briefly, the no-penetration-boundary condition may be enforced, to yield

$$\alpha_{\text{eff}} = \alpha_{\text{geo}} - \alpha_i \tag{5}$$

where α_{eff} represents downwash associated with the wing's bound vortex system, and α_i is the downwash associated with the trailing vortex sheet. Substitution of describing equations for α_{eff} and α_i yields

$$\alpha(y_o) = \frac{\Gamma(y_o)}{\pi U c(y_o)} + \alpha_{\text{ZL}}(y_o) + \frac{1}{4\pi U}\int_{-b/2}^{b/2} \frac{(\mathrm{d}\Gamma/\mathrm{d}y)}{(y_o - y)}\,\mathrm{d}y \tag{6}$$

where y_o is the point of interest at which the effects of the wing's bound and trailing vortex system are evaluated; y_o is then varied across the span. Equation (6) is solved numerically by assuming a spanwise load distribution that is represented by a Fourier series; solution involves determination of the Fourier coefficients. Equation (6) transforms into

$$\alpha(\phi_o) = \frac{2b}{\pi c(\phi_o)}\sum_{1}^{N} A_n \sin n\phi_o + \alpha_{\text{ZL}}(\phi_o) + \sum_{1}^{N} \frac{nA_n \sin n\phi_o}{\sin n\phi_o} \tag{7}$$

where the subscript o indicates the point of evaluation corresponding to a specific spanwise station. Evaluation of Eq. (7) at N spanwise locations leads to a set of N-independent equations that are solved for the A_n. To determine the wing's lift coefficient, only the first Fourier coefficient, A_1, is required ($C_L = A_1\pi\text{AR}$). The rolling moment may be determined from $C_l = A_2\pi\text{AR}/4$ or may simply be evaluated by integrating the sectional moment, due to the lift across the span.

For symmetrical flow conditions, it is only necessary to evaluate the equation over one wing half: ϕ ranging from 0 to $\pi/2$. However, a deflected aileron represents an asymmetric condition; thus, the circulation was determined by varying ϕ from 0 to π (i.e., across the whole span). The effect of the ailerons was estimated by setting the zero lift angle α_{ZL} to be positive on one wing half (i.e., an upward deflected aileron) and negative on the other wing half in the spanwise region in which the aileron is located. Typically, most implementations of numerical lifting-line theory use a cosine spanwise distribution of points at which to evaluate the Fourier coefficients (using the transformation $y = -b/2\cos\phi$). This promotes accuracy by packing in points at which spanwise gradients are the largest (the wing tip). However, for a deflected aileron that is only a partial span, it is necessary to have significant point density in the spanwise vicinity of the aileron. Consequently, a linear point distribution was used, such that $y = -(b/2)\phi$. Sufficient terms in the Fourier series were used to ensure accuracy.

Figure 9 shows a comparison between spanwise load estimates from the lifting-line program and a vortex-lattice lifting-surface code (200 panels) for a wing typical of that seen on a one-third-scale Extra 330S aircraft (symmetrical conditions). Note that the AR of this wing is at the low end of what may be considered applicable for lifting-line analysis (due to this formulation ignoring chordwise loading effects). However, as may be seen, the lifting-line program shows encouraging agreement with the lifting-surface theory, although accord does reduce near the wing tips.

Figure 10 shows the estimated rolling moment coefficient for a common spanwise aileron extent and location (these dimensions will also be used in the hingeless roll control flight vehicle). Also included for comparison are moment estimates assuming a 10 and 20% aileron deflection at the specified location (the zero lift angle of attack was estimated using a Smith–Hess panel method with 100 panels on the top and 100 panels on the lower surface). The results indicate that the Gurney/jet flap actuator is capable of generating rolling moments that are sufficient for significant roll control and increase approximately linearly with the jet momentum coefficient. It is also evident that a minimally structurally significant flow effector

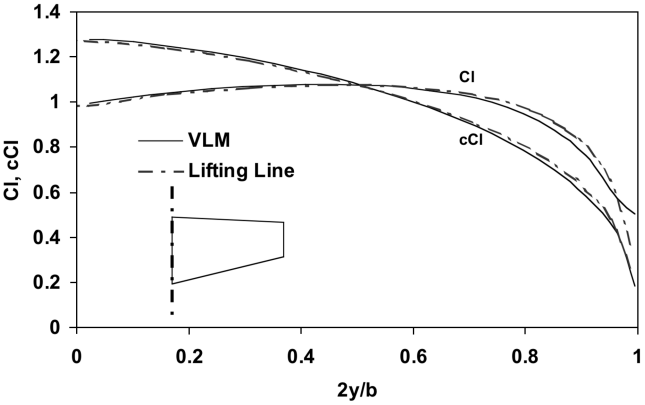

Fig. 9 Comparison of spanwise loading estimated using numerical lifting-line theory and a vortex lattice method (200 panels). The wing is that of an Extra 330S R/C aircraft, with AR = 5, a span of 2.45 m, root chord of 0.646 m, tip chord of 0.355 m, and a wing area of 1.225 m^2.

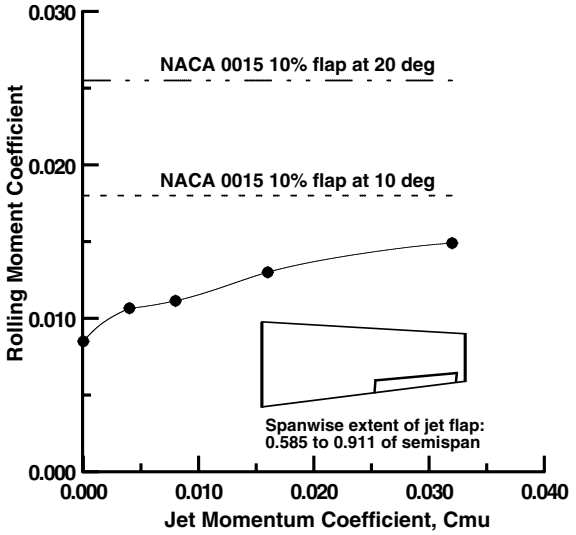

Fig. 10 Estimated rolling moment due to the jet flap and conventional trailing-edge flap.

such as a Gurney flap is capable of generating significant rolling moments, which may prove valuable for stealth application.

Effective Aileron Location

For the purpose of hingeless control (or any other), it is useful to have an estimate of the optimal spanwise location for the ailerons to maximize their control power. It is commonly held that the most effective location for an aileron is at the wing tip, due to this location possessing the maximum moment arm. However, downwash effects from the wing tip vortex reduces the loading near the tip and reduces the aileron effectiveness. Thus, maximum flap effectiveness was estimated for a simple generic unswept rectangular wing (AR = 5). The location for maximum flap aileron effectiveness may be estimated using Eq. (7) or the semi-empirical method detailed in [16]. Both methods yielded essentially the same result. Estimates for the rolling moment developed (normalized by the rolling moment with the aileron located with its outboard extent at the wing tip) are shown in Fig. 11. Data are presented for two aileron extents: 20 and 40% of the semispan. The estimates suggest that the optimal location for the center of the aileron is at approximately 65% of the semispan for both aileron sizes. The data also suggest that a smaller-span aileron is more sensitive to location, for optimal effectiveness.

Jones and Cohen [17] conducted a theoretical study to determine the optimum planform for control surfaces. A figure from this report is reproduced as Fig. 12. The spanwise station $2y/b$ indicates the extent of the aileron from the wing tip. The aileron is assumed to start

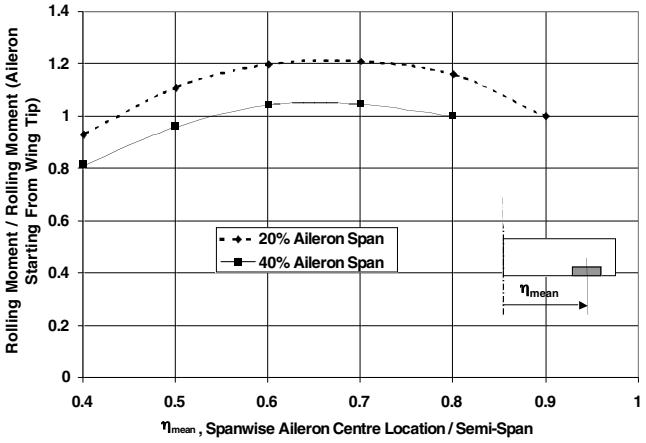

Fig. 11 Effect of aileron location on the rolling moment ratio (unswept rectangular planform).

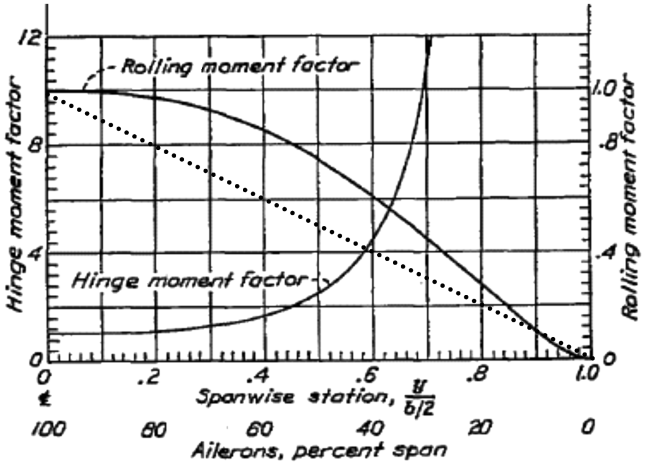

Fig. 12 Effect of aileron extent on the rolling moment factor; figure reproduced from [17].

from the wing tip in all cases. The rolling moment factor is the calculated rolling moment for the partial-span aileron, divided by the rolling moment from a full-span aileron. What the plot indicates is that a short aileron (less than 10% semispan) located at the tip is inefficient (due to wing tip downwash effects). However, the aileron effectiveness is considerably greater than its spanwise extent (indicated by the curve's location above the straight line). For example, an aileron at 40% of the semispan generates a rolling moment at 60% of the value that would be achieved using full-span ailerons.

Conclusions

A Gurney/jet flap combination has been evaluated as a possible control effector for generating rolling moments on an unmanned aerial vehicle type configuration. A low-speed wind-tunnel study incorporating force balance, wake survey, and flow visualization was undertaken. The results show that even at low Reynolds numbers, the theoretical dependencies of the performance of the jet flap on its momentum coefficient are maintained. To estimate the ability of the Gurney/jet flap to generate moments sufficient for lateral control, a modified lifting-line procedure was implemented. The numerical results indicate that using feasible jet momentum coefficients, rolling moments of sufficient magnitude for control may be generated.

References

[1] Spence, D. A., "Some Simple Results for Two-Dimensional Jet-Flap Aerofoils," *The Aeronautical Quarterly*, Nov. 1958, pp. 395–406.

[2] Jeffrey, D., Zhang, X., and Hurst, D. W., "Aerodynamics of Gurney Flaps on a Single-Element High-Lift Wing," *Journal of Aircraft*, Vol. 37, No. 2, 2000, pp. 295–301.

[3] Papadakis, M., Myose, R. Y., Heron, I., and Johnson, B. L., "An Experimental Investigation of Gurney Flaps on a GA(W)-2 Airfoil with 25% Slotted Flap," AIAA Paper 96-2437, 1996.

[4] Liebeck, R. H., "Design of Subsonic Airfoils for High Lift," *Journal of Aircraft*, Vol. 15, No. 9, 1978, pp. 547–561.

[5] Meyer, R., Hage, W., Bechert, D. W., Schatz, M., Thiele, F., "Drag Reduction on Gurney Flaps by Three-Dimensional Modifications," *Journal of Aircraft*, Vol. 43, No. 1, 2006, pp. 132–140.

[6] Traub, L. W., Miller, A., and Rediniotis, O., "Preliminary Parametric Study of Gurney-Flap Dependencies," *Journal of Aircraft*, Vol. 43, No. 4, 2006, pp. 1242–1244.

[7] Jones, B. M., "Measurement of Profile Drag by the Pitot-Traverse Method," Aeronautical Research Council, Reports and Memoranda No. 1688, 1936.

[8] Myose, R., Heron, I., and Papadakis, M., "Effects of Gurney Flaps on a NACA 0011 Airfoil," AIAA Paper 96-0059, Jan. 1996.

[9] Zerihan, J., and Zhang, X., "Aerodynamics of Gurney Flaps on a Wing in Ground Effect," *AIAA Journal*, Vol. 39, No. 5, 2001, pp. 772–780.

[10] Hoerner, S. F., *Fluid-Dynamic Drag*, Hoerner Fluid Dynamics, Vancouver, WA, 1965, pp. 3-19–3-21.

[11] Hoerner, S. F., *Fluid-Dynamic Lift*, Hoerner Fluid Dynamics, Vancouver, WA, 1985, pp. 2–11.

[12] Jordinson, R., "Flow in a Jet Directed Normal to the Wind," Aeronautical Research Council, Reports and Memoranda No. 3071, Oct. 1956.

[13] Traub, L. W., Miller, A., and Rediniotis, O., "Comparisons of a Gurney and Jet-Flap for Hinge-Less Control," *Journal of Aircraft*, Vol. 41, No. 2, 2004, pp. 420–423.

[14] Houghton, E. L., and Carpenter, P. W., *Aerodynamics for Engineering Students*, Butterworth–Heinemann, Oxford, 2003, pp. 249–255.

[15] Anderson, J. D., *Fundamentals of Aerodynamics*, McGraw–Hill, New York, 2001, pp. 371–375.

[16] Anon., "ESDU 88013," Engineering Science Data Unit, London, 1992.

[17] Jones, R. T., and Cohen, D., "Determination of Optimum Plan Forms for Control Surfaces," NACA Rept. 731, Jan. 1941.